Available online at www.sciencedirect.com

SciVerse ScienceDirect

Ceramics International 38 (2012) 6729–6738

CERAMICS INTERNATIONAL

www.elsevier.com/locate/ceramint

Synthesis of calcium phosphate-based composite nanopowders by mechanochemical process and subsequent thermal treatment

Abbas Fahami*, Bahman Nasiri-Tabrizi, Reza Ebrahimi-Kahrizsangi

Materials Engineering Department, Najafabad Branch, Islamic Azad University, Najafabad, Isfahan, Iran

Received 5 April 2012; received in revised form 12 May 2012; accepted 22 May 2012
Available online 6 June 2012

Abstract

One-step mechanochemical process followed by thermal treatment has been used to produce calcium phosphate-based composite nanopowders. Effects of milling and subsequent heat treatment on the phase transition as well as structural features were investigated. The products were characterized by powder X-ray diffraction (XRD), Fourier transform infrared (FT-IR) spectroscopy, scanning electron microscopy (SEM), energy dispersive X-ray spectroscopy (EDX), and transmission electron microscopy (TEM) techniques. The results revealed that the dominant phases after mechanical activation were hydroxyapatite, anatase (TiO_2), and periclase (MgO), while after thermal annealing process at 700 °C hydroxyapatite along with geikielite ($MgTiO_3$) and periclase (MgO) were the major phases. In addition, decomposition of hydroxyapatite to tricalcium phosphate (β-TCP) occurred after heat treatment in the range 900–1100 °C which resulted in the formation of tricalcium phosphate-based composite nanopowders. Evaluation of structural features of the samples calculated by X-ray diffraction profiles analysis indicated that the average crystallite size of hydroxyapatite after 10 h of milling and subsequent heat treatment at 700 °C were about 21 and 34 nm, respectively. TEM and SEM studies exhibited that the considerable morphological changes at temperatures ≥ 900 °C had to be ascribed not only to grain growth, but also for the transformation of hydroxyapatite to β-TCP.

Keywords: Mechanochemical; Calcium phosphate; $MgTiO_3$; Structural features

1. Introduction

The recent trend in bioceramic research is predominantly focused on calcium phosphate-based materials, as they exhibit superior biological and mechanical properties over other materials [1–3]. Among different calcium phosphates, hydroxyapatite (HAp, $Ca_{10}(PO_4)_6(OH)_2$) and β-tricalcium phosphate (β-TCP, $Ca_3(PO_4)_2$) have been considerably employed in the biomedical fields due to their biocompatibility and osteoconductivity [4]. From a thermodynamic standpoint, HAp is the most stable phase in physiological conditions and has the ability for direct chemical bonding to the bone, while β-TCP is found to be resorbable in vivo with new bone growth replacing the implanted β-TCP [5]. According to literature [6], β-TCP is an effectual implant in accelerating the formation of new bone owing to the solubility and biodegradation rate of β-TCP and are much higher than those of HAp.

However, these bioceramics have inherently some weaknesses such as poor toughness and low bending strength, poor corrosion resistance in an acid environment, and poor chemical stability at high-temperatures which have restricted wider applications in the fields of orthopedic and dentistry [7–9]. Therefore, improvements on structural features as well as mechanical properties of calcium phosphates have been attempted in a number of studies [10–12]. Theoretical and experimental investigations have shown that such properties of calcium phosphates can be remarkably strengthened by various methods, such as making nanocomposites [13], use of different sintering techniques [14], and adding dopants [11]. In the field of nanocomposites, an ideal reinforcing material for calcium phosphate-based composites has not yet been found. Nevertheless, different approaches have been extensively investigated in order to develop calcium phosphate-based

*Corresponding author. Tel.: +98 3114437009; fax: +98 3312291008.
E-mail address: ab.fahami@gmail.com (A. Fahami).

0272-8842/$36.00
http://dx.doi.org/10.1016/j.ceramint.2012.05.064

composites, for instance HAp-Al_2O_3 [15], HAp-ZrO_2 [16], HAp-TiO_2 [17], poly(lactide-co-glycolide)/β-TCP [18], polyglycolic acid (PGA)/β-TCP [19], and TiO_2/TCP [20] composites. These studies exhibited that interfacial reactions occurred during the high temperature processing of composites due to the large interfacial area available for the reactions. Interfacial reactions result in the formation of new phases, influence densification, mechanical properties and even degrade the biological properties of the composite in some cases which often limit their performance [15]. Hence, production and characterization of novel HAp/$MgTiO_3$–MgO and β-TCP/$MgTiO_3$–MgO composite nanopowders provided the main target for current research. It should be noted that despite a large number of studies on the synthesis of HAp and TCP composites [15–20], no systematic investigations on the preparation of HAp/$MgTiO_3$–MgO and β-TCP/$MgTiO_3$–MgO are performed. Over the past decades, various synthesis methods of such biomaterials have been reported, including wet chemical methods [21,22], hydrothermal processes [23], solid-state reaction [24], and the sol-gel method [25]. Among them, mechanochemical process has been extended for the production of a wide range of advanced materials [26,27]. The prominent features of this technique are that melting is not essential and that the products have nanostructural characteristics [24].

In this paper, mechanosynthesis of calcium phosphate-based materials was investigated. In addition, effect of subsequent heat treatment on the phase transformation was evaluated. Since nanostrutured calcium phosphate composite nanopowders with appropriate stoichiometry, high purity and crystallinity enhance densification, osseointegrative, and bioactive properties [5], structural features (crystallite size, lattice strain, and crystallinity) as well as morphological characteristics (particle size and shape, particle distribution and agglomeration) of composite nanopowders were investigated by using XRD, FT-IR, SEM/EDX and TEM techniques.

2. Experimental procedures

2.1. Composite preparation

The starting reactant materials were anhydrous calcium hydrogen phosphate ($CaHPO_4$, Merck, Germany), calcium oxide (CaO, Merck, Germany), titanium dioxide (TiO_2, Merck, Germany), and magnesium (Mg, Merck, Germany). Synthesis of calcium phosphate-based composite nanopowders consists of (i) mechanical activation of powder mixture and (ii) subsequently thermal treatment. For this purpose, anhydrous calcium hydrogen phosphate and calcium oxide powder mixture with Ca/P ratio = 1.67 mixed with distinct amount of elemental magnesium and titanium dioxide powder blend (20 wt%) with Mg/Ti ratio = 2. Afterwards, the obtained mixture was milled in a high energy planetary ball mill for 10 h according to the following reaction.

$$6CaHPO_4 + 4CaO + TiO_2 + 2Mg \rightarrow Ca_{10}(PO_4)_6(OH)_2 + TiO_2 + 2MgO + 2H_2 \uparrow \quad (1)$$

Mechanical activation was carried out in polyamide-6 vial using Zirconia balls (diameter 20 mm). The ball-to-powder weight ratio and milling speed were 20:1 and 600 rpm, respectively. It should be mentioned that the total powder mass was 6 g. Finally, the milled powders were heat treated under air atmosphere at 700, 900, and 1100 °C for 2 h. Details of process specifications and abbreviated name of products are given in Table 1.

2.2. Characterization techniques

The phase composition of powders was investigated using X-ray diffraction (Philips X-ray diffractometer) with *Cu Kα* radiation at 40 kV and 30 mA. During X-ray diffractometry, the step size was 0.05°. All measurements were performed at room temperature with the diffraction range of $2\theta = 20–60°$. In this paper, the *PANalytical X'Pert HighScore* software was used for the analysis of the different peaks. The diffraction patterns of samples were compared to standards compiled by the Joint Committee on Powder Diffraction and Standards (JCPDS), which involved card # 09–0432 for HAp, # 09–0169 for β-TCP, # 04–0829 for MgO, # 071–1166 for TiO_2, # 06–0494 for $MgTiO_3$, and # 017–0912 for CaO. Average crystallite size and lattice strain of the samples were determined by using the XRD data according to the following equations [26]:

$$D = \frac{K\lambda}{(b_{obs} - b_{std})(b\cos\theta)} \quad (I)$$

$$E^2 = \frac{(b_{obs}{}^2 - b_{std}{}^2)}{(4\tan\theta)^2} \quad (II)$$

Table 1
Specifications of the synthesis process and abbreviated name of specimens.

Series	Composition	Process
I	100 wt% ($CaHPO_4$,CaO)	Milling (10 h)
II	80 wt% ($CaHPO_4$, CaO)+20 wt% (TiO_2,Mg)	Milling (10 h)
III	80 wt% ($CaHPO_4$, CaO)+20 wt% (TiO_2,Mg)	Milling (10 h)+annealing (700 °C for 2 h)
IV	80 wt% ($CaHPO_4$, CaO)+20 wt% (TiO_2,Mg)	Milling (10 h)+annealing (900 °C for 2 h)
V	80 wt% ($CaHPO_4$, CaO)+20 wt% (TiO_2,Mg)	Milling (10 h)+annealing (1100 °C for 2 h)

where b (rad) is the structural broadening, which is the difference in integral profile width between a standard and the unknown sample and K, λ, D, E, and θ are the shape coefficient (value between 0.9 and 1.0), the wavelength of the X–ray used (0.154056 nm), crystallite size, lattice strain, and the Bragg angle (°), respectively.

On the other hand, the fraction of crystalline phase (Xc) in HAp and β-TCP was evaluated by the following equation [28]:

$$Xc = \left(\frac{K}{B}\right)^3 \quad \text{(III)}$$

where K and B are a constant found equal to 0.24 and FWHM (°) of selected reflection peaks, respectively. It should be noted that the average of fraction of crystalline phase (Xc) in HAp and β-TCP was determined by using the two groups of peaks; one group was (211), (112) and (300) which related to HAp, and another was (1010), (214) and (0210) which corresponded to β-TCP.

The functional groups of products were examined by Fourier transform infrared (FT-IR: Bruker TENSOR27, Germany) in the range of $4000-400\,cm^{-1}$. For this purpose, 1 mg of the sample was mixed with appropriate amount of spectroscopic grade KBr by hand milling the powder in an agate mortar. Energy dispersive X-ray spectroscopy (EDX) which is coupled to SEM was used for the semi-quantitative test of the products. The morphological characteristics of the samples which sputter-coated with a thin layer of gold was examined by scanning electron microscope (SEM, SERON AIS-2100, The South Korean). The size and morphology of fine powders as well as crystal growth at high temperature (1100 °C) were surveyed in a transmission electron microscope (Philips CM10, Eindhoven, The Netherlands) which operates at 100 kV.

3. Results and discussions

3.1. XRD analysis

3.1.1. Phase determination

Fig. 1 shows the XRD spectra of the samples after mechanical activation and subsequent thermal treatment at different temperatures. The pattern for sample I (Fig. 1a) shows well characterized peaks of pure HAp and the peaks were indexed according to the standard pattern (JCPDS 09–0432). In this sample, diffraction peaks broadened, particularly $2\theta = 31–35°$, indicating that the sample demonstrated poor crystallinity (low fraction of crystalline phase). Therefore, the product of mechanochemical process (reaction 2) between $CaHPO_4$ and CaO was pure HAp according to the following reaction.

$$6CaHPO_4 + 4CaO \rightarrow Ca_{10}(PO_4)_6(OH)_2 + 2H_2O\uparrow \quad (2)$$

The peaks in the spectrum for sample II (Fig. 1b) correspond to HAp as a major phase with anatase (TiO_2) and periclase (MgO) as minor phases. This indicated that the product of mechanochemical process in presence of 20 wt% (TiO_2, Mg) was HAp/MgO–TiO_2 composite. From Fig. 1c it was verified the existence of HAp and geikielite ($MgTiO_3$) phases together with minor MgO phase after the annealing at 700 °C. It is clearly seen that

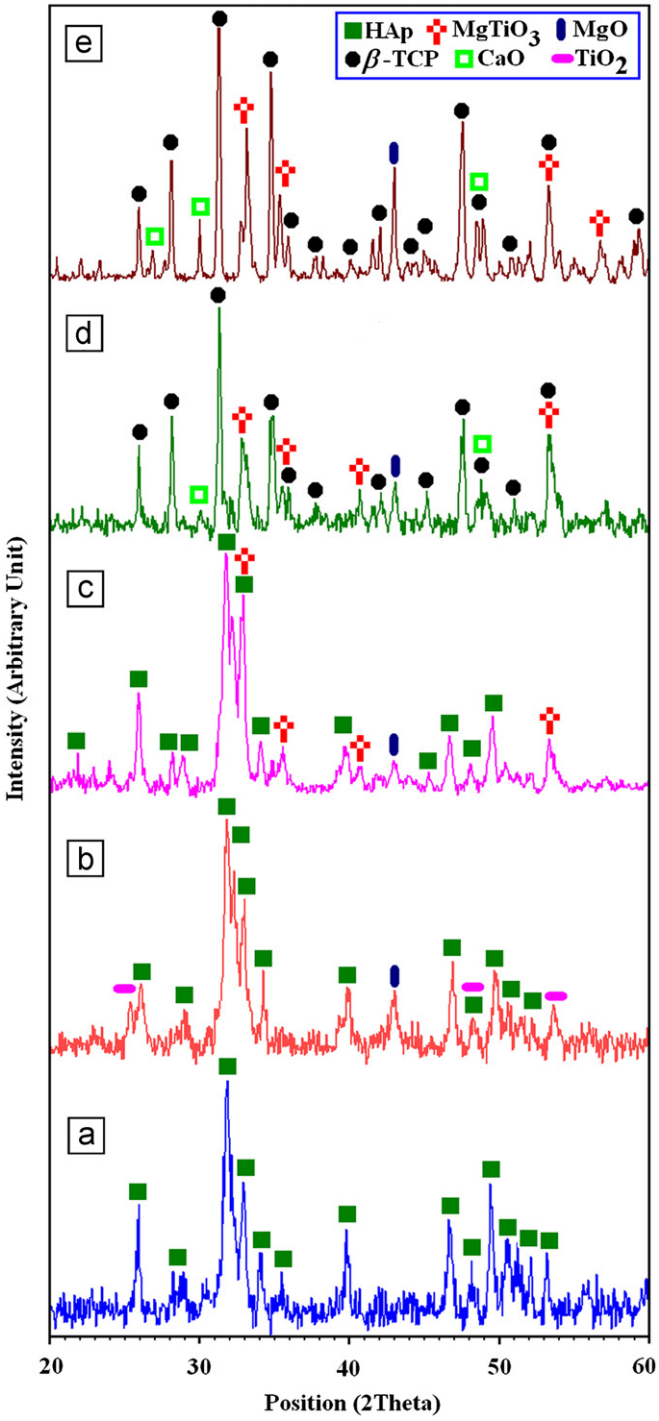

Fig. 1. XRD patterns of the samples: (a) HAp after 10 h of milling, (b) HAp/TiO_2–MgO after 10 h of milling, (c) HAp/$MgTiO_3$–MgO after 10 h of milling+heat treatment at 700 °C, (d) β-TCP/$MgTiO_3$–MgO after 10 h of milling+heat treatment at 900 °C, and (e) and β-TCP/$MgTiO_3$–MgO after 10 h of milling+heat treatment at 1100 °C.

the thermal treatment at 700 °C led to the formation of $MgTiO_3$ by the following reaction:

$$MgO + TiO_2 \rightarrow MgTiO_3 \qquad \Delta G_{298\,K} = -25.410\ \text{kJ},\ \Delta H_{298\,K} = -26.209\ \text{kJ} \tag{3}$$

According to Fig. 1(d) and (e), thermal treatment in the range 900–1100 °C caused the formation of β-TCP/$MgTiO_3$–MgO composite. However, the peaks associated with HAp disappeared and several peaks corresponding to the high crystalline β-TCP phase emerged as the annealing temperature increased from 700 °C to 1100 °C. This indicates that HAp can be decomposed into β-TCP and CaO at temperatures above 700 °C by the following reaction:

$$Ca_{10}(PO_4)_6(OH)_2 \rightarrow 3Ca_3(PO_4)_2 + CaO + H_2O \tag{4}$$

It was reported [12] that the decomposition temperature (600–800 °C) strongly depends on the preparation method of the HAp powder. Thus, the annealing temperature must be selected ≤ 700 °C if the purpose is to achieve pure HAp without any extra biocompatible phase presentation. It was found that MgO-doped HAp/TCP ceramics present high density and significantly enhance the mechanical properties without any phase transformation of β-TCP to α-TCP up to 1300 °C [2]. Moreover, a patent [29] reported the biocompatibility and osteoconductivity of magnesium titanate oxide film implant for utilizing in several medical fields such as dentistry, orthopedic, maxillofacial, and plastic surgery. Therefore, the presence of MgO and $MgTiO_3$ phases along with HAp and/or TCP in outputs can enhance the biological and mechanical properties of calcium phosphate-based materials. From all these results, we reach to an important conclusion that applying appropriate mechanochemical process and subsequent thermal treatment caused the formation of calcium phosphate-based nanocomposites which may improve the structural features as well as morphological properties of calcium phosphates. In section 3.1.2 we provide a brief overview of the structural features of the samples.

3.1.2. Structural features

In order to investigate the effect of milling and subsequent thermal treatment on the formation of crystalline phases, the fraction of the crystalline phase of the specimens was determined by using the XRD profiles. Fig. 2 shows variation in XRD profiles in 3D view mode for samples during milling and after thermal treatment in the range 700–1100 °C. In this paper, crystallinity was expressed in accordance with the line broadening at the (211), (112) and (300) diffraction peaks for HAp and (1010), (214) and (0210) diffraction peaks for β-TCP. As can be seen in Fig. 2a–c, poor crystalline apatite phase was obtained after 10 h of milling (sample I), while in presence of 20 wt% elemental magnesium and titanium dioxide powder blend (sample II) the crystallinity rapidly increased and the fraction of crystalline phase of HAp reached about 0.54. Finally, high crystalline HAp-based composite was produced after annealing at 700 °C (sample III). On the other hand, the existence of β-TCP phase was confirmed after the annealing at temperatures above 900 °C as shown in Fig. 2d–f. This indicated that an absolute decomposition of HAp occurred in the range 900 − 1100 °C. The fraction of crystalline phase of β-TCP sharply increased at 900 °C and strongly recovered at 1100 °C. After 1100 °C, the fraction of crystalline phase of β-TCP was about 1.4. It has been reported [17] that the final microstructure of TCP will contain β or α − TCP depending on their cooling rates. Rapid cooling from sintering temperature gives rise to α-TCP phase only, whereas slow furnace cooling leads to β-TCP phase only. Any moderate cooling rate, in between these two results lead to mixed phase of both β and α-TCP. However, in the present investigation the slow furnace cooling rate led to the formation of β-TCP phase in the heat treated samples (≥ 900 °C).

Since crystallinity is principally determined by the two main factors of crystallite size and residual elastic strain, the average crystallite size and lattice strain of the samples were examined (Table 2). Based on Table 2, the lattice strain in HAp powder rapidly increased and reached about 0.604% after 10 h of milling. The low fraction of crystalline phase of HAp was due to the crystal strain and refinement of crystals. On the contrary, the breadth of fundamental diffraction peaks decreased after the heat treatment as compared to the results for the milled powder. This phenomenon can be attributed to an increase in the fraction of crystalline phase due to an increase of crystallite size and a decrease of lattice strain. The calculated amounts of structural features indicated that increasing the annealing temperature might assist grain growth although all the composite powders were comprised of nanosize crystallites. Hence, annealing temperature plays an important role on structural features of calcium phosphate-based nanocomposites.

3.2. FT-IR evaluation

FT-IR is a favorable instrument to recognize unknown substances and to determine the amount of components in a given sample. This test was accomplished to get authenticated information about the vibrational origin of the phosphate and carbonate groups and to confirm the production of calcium phosphate-based materials with no association of organic moieties [30,31]. According to the literature [2,12,13,17,24,30,31], the functional groups generally observed in the FT-IR spectra of calcium phosphate-based materials are PO_4^{3-}, OH^-, CO_3^{2-}, and HPO_4^{2-} groups in the range $4000 - 300\ cm^{-1}$. Phosphate group (PO_4^{3-}) appear at around $1100 - 1019\ cm^{-1}$ for the v_3 mode, $958\ cm^{-1}$ for the v_1 mode, $605 - 530\ cm^{-1}$ for the v_4 mode, and $500 - 400\ cm^{-1}$ for the v_2 mode. Furthermore, three modes of OH^- ions, i.e. stretching, vibrational, and translational modes are at $3700 - 2500$, 630, and $390\ cm^{-1}$, respectively. The band of HPO_4^{2-} ions emerged at

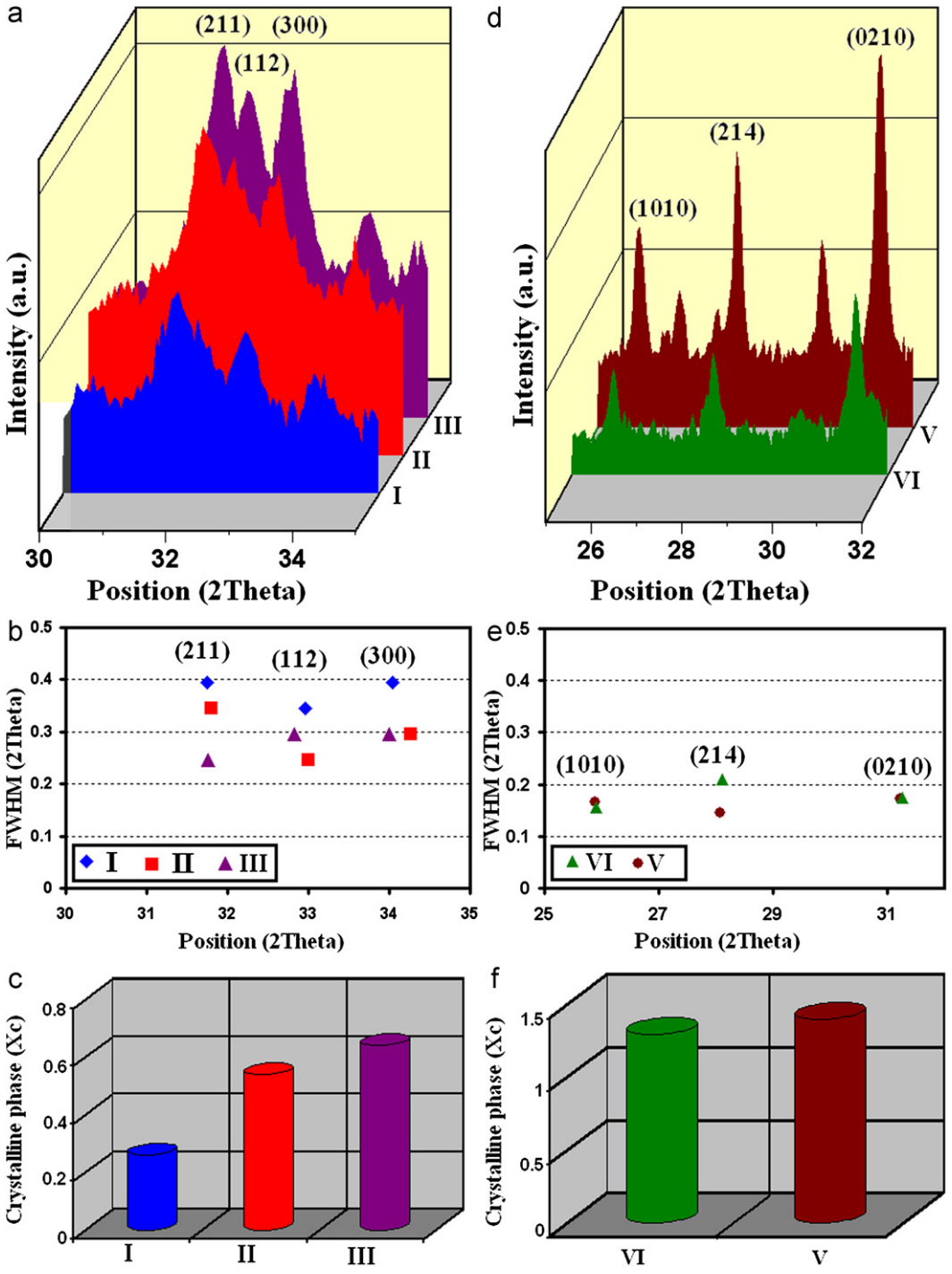

Fig. 2. Variation in XRD profiles in 3D view mode for samples during milling and after thermal treatment in the range of 700–1100 °C.

Table 2
Average crystallite size and lattice strain of the samples before and after thermal treatment.

Series	MT (h)	Temperature (°C)	*D* (nm)				*E* (%)			
			HAp	TCP	MgO	$MgTiO_3$	HAp	TCP	MgO	$MgTiO_3$
I	10	–	21.3	–	–	–	0.604	–	–	–
II	10	–	24.4	–	10.8	–	0.527	–	0.884	–
III	10	700	34.4	–	17.6	13.2	0.377	–	0.545	0.871
IV	10	900	–	43.3	29.5	20.3	–	0.339	0.327	0.386
V	10	1100	–	51.9	44.7	58.3	–	0.268	0.218	0.238

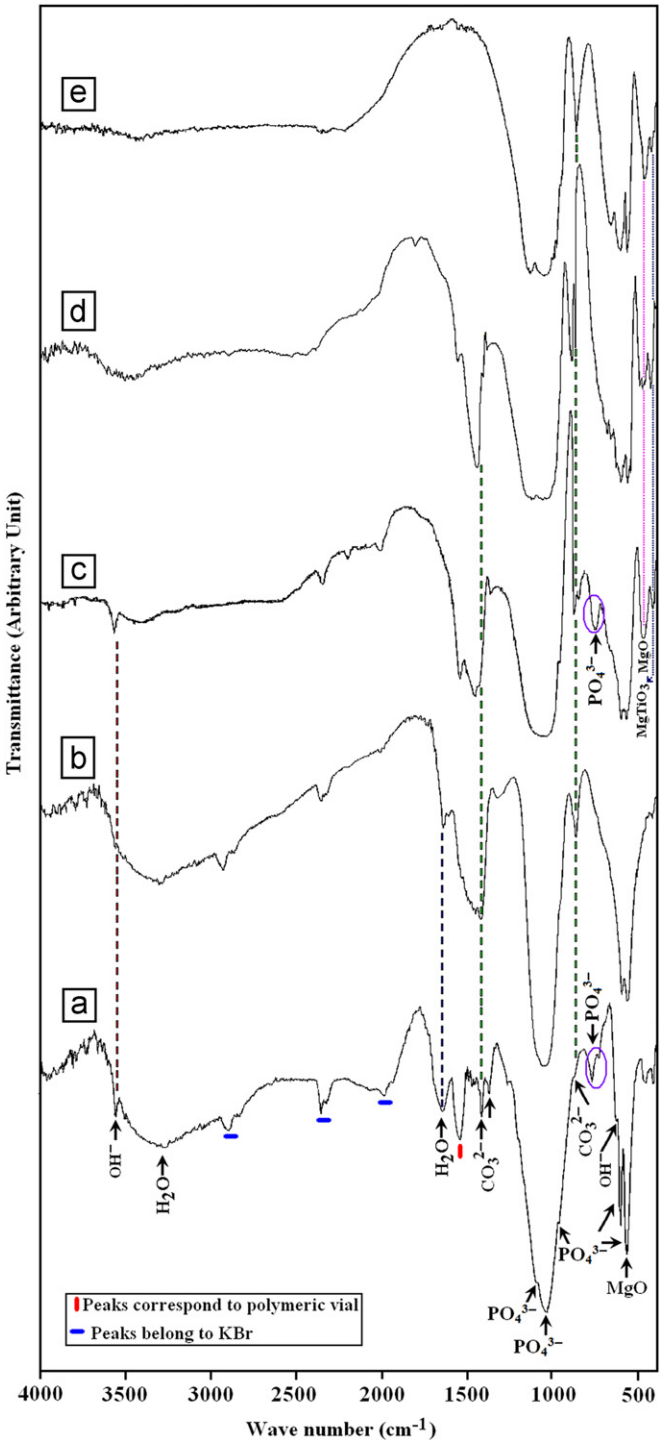

Fig. 3. FT-IR spectra of the samples: (a) HAp after 10 h of milling, (b) HAp/TiO_2–MgO after 10 h of milling, (c) HAp/$MgTiO_3$–MgO after 10 h of milling + heat treatment at 700 °C, (d) β-TCP/$MgTiO_3$–MgO after 10 h of milling + heat treatment at 900 °C, and (e) and β-TCP/$MgTiO_3$–MgO after 10 h of milling + heat treatment at 1100 °C.

875 cm^{-1}. However, overtone and combination of the v_3 and v_1 modes of phosphate group or even HPO_4^{2-} may be emerged. It should be noted that the water molecules appear at 1642 cm^{-1} which may be obscured by the CO_3^{2-} bands.

Table 3
Characteristic infrared bands of HAp, HAp- and β-TCP-based composites.

S. No.	Vibrational frequency (cm^{-1})	Assignments
1	1645, 3300–3800	H_2O
2	1419, 1458, and 1475	$v_3(CO_3^{2-})$
3	873	$v_2(CO_3^{2-})$
4	628	OH^-
5	1031 and 1089	$v_3(PO_4^{3-})$
6	960	$v_1(PO_4^{3-})$
7	565 and 602	$v_4(PO_4^{3-})$
8	466	$v_2(PO_4^{3-})$
9	570 and 443	Mg–O vibrations
10	675 and 459	A_u mode corresponding to $MgTiO_3$
11	557 and 422	E_u mode corresponding to $MgTiO_3$
12	500–800 cm^{-1}	Ti–O vibration bands
13	2000, 2350, and 2931	KBr

Fig. 3 shows the FT-IR spectra of the HAp, HAp- and β-TCP-based composite nanopowders which were produced after 10 h of milling and subsequent heat treatment. The predominant characteristic of the FT-IR bands was presented in Table 3. Based on Fig. 3 and Table 3, phosphate ions ($PO4^{3-}$) had four distinct asymmetrical stretching vibration modes, namely, v_1, v_2, v_3, and v_4. The v_1 and v_2 vibration peaks were observed at 960 and at 466 cm^{-1}, respectively. As a major peak of the phosphate group, the v_3 vibration peaks were detected in the region between 1089 and 1031 cm^{-1}. The band between 602 and 565 cm^{-1} exhibited the v_4 vibration mode of the phosphate group. Besides, on heating at $\geq$900 °C, a new peak at 972 cm^{-1} corresponding to phosphate group appeared which confirmed the formation of β-TCP [2], as indicated from the X-ray patterns. The peaks observed at 1419, 1458, and 1475 cm^{-1} in the spectra of the samples attributed to $v_3(CO_3^{2-})$. In addition, the band at 873 cm^{-1} corresponding to v_2 vibration mode of carbonated groups was observed. These peaks showed that the products contained some CO_3^{2-} groups in PO_4^{3-} sites of the apatite lattice (B-type substitution) [12,13,31]. Since carbonates are constituents of hard tissue structures [32], the presence of low content of CO_3^{2-} can improve the bioactivity of calcium phosphate-based materials. A relatively broad band stretch over the range 3300–3800 cm^{-1} correlating to the adsorbed molecules of water was detected [2]. Also, the band at 1645 cm^{-1} allocates to water molecules which is probably because the mixtures had absorbed some water during the investigative process [31]. On the other hand, the bands at 570 and 443 cm^{-1} as MgO vibrations were detected [33]. It was found that $MgTiO_3$ has eight FT-IR active modes [34]. In this paper, four modes were observed in the region 680–420 cm^{-1}. The remaining four FT-IR bands take place below 400 cm^{-1}. The bands detected, in the present study, were 675 cm^{-1} (A_u), 557 cm^{-1} (E_u), 459 cm^{-1} (A_u), and 422 cm^{-1} (E_u), which are in good agreement with other reports [33,34]. However,

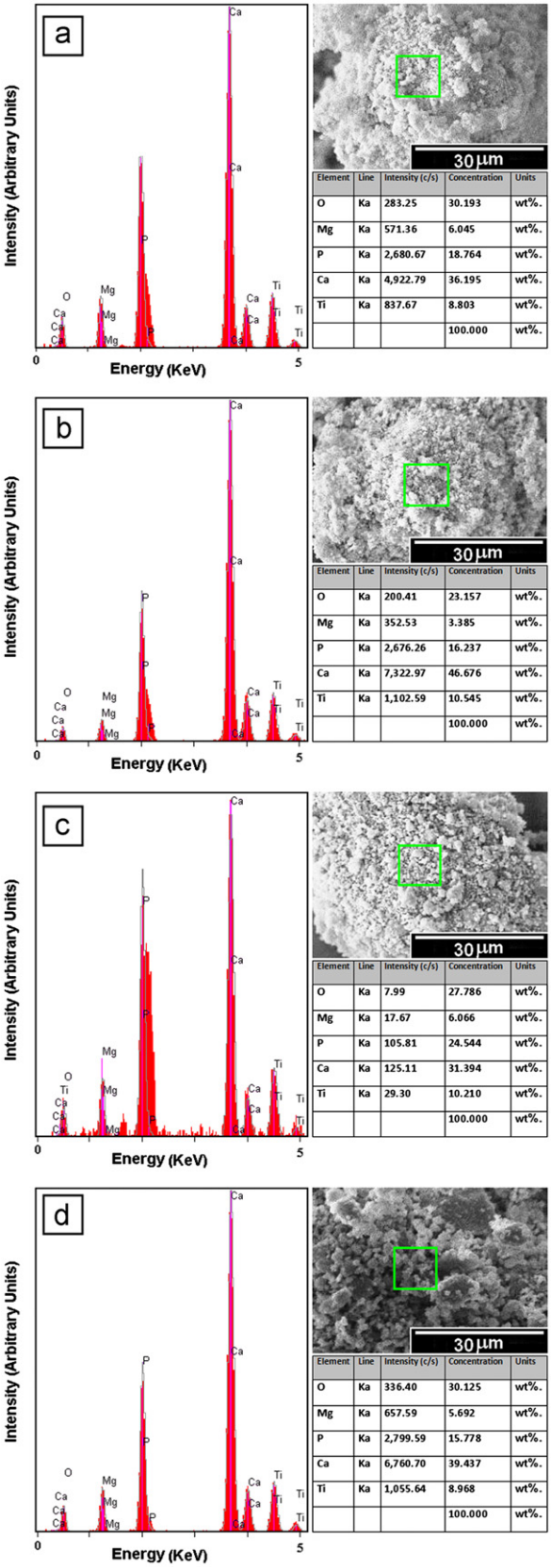

Fig. 4. EDX results of the samples: (a) HAp/TiO_2–MgO after 10 h of milling, (b) HAp/$MgTiO_3$–MgO after 10 h of milling+heat treatment at 700 °C, (c) β-TCP/$MgTiO_3$–MgO after 10 h of milling+heat treatment at 900 °C, and (d) β-TCP/$MgTiO_3$–MgO after 10 h of milling+heat treatment at 1100 °C.

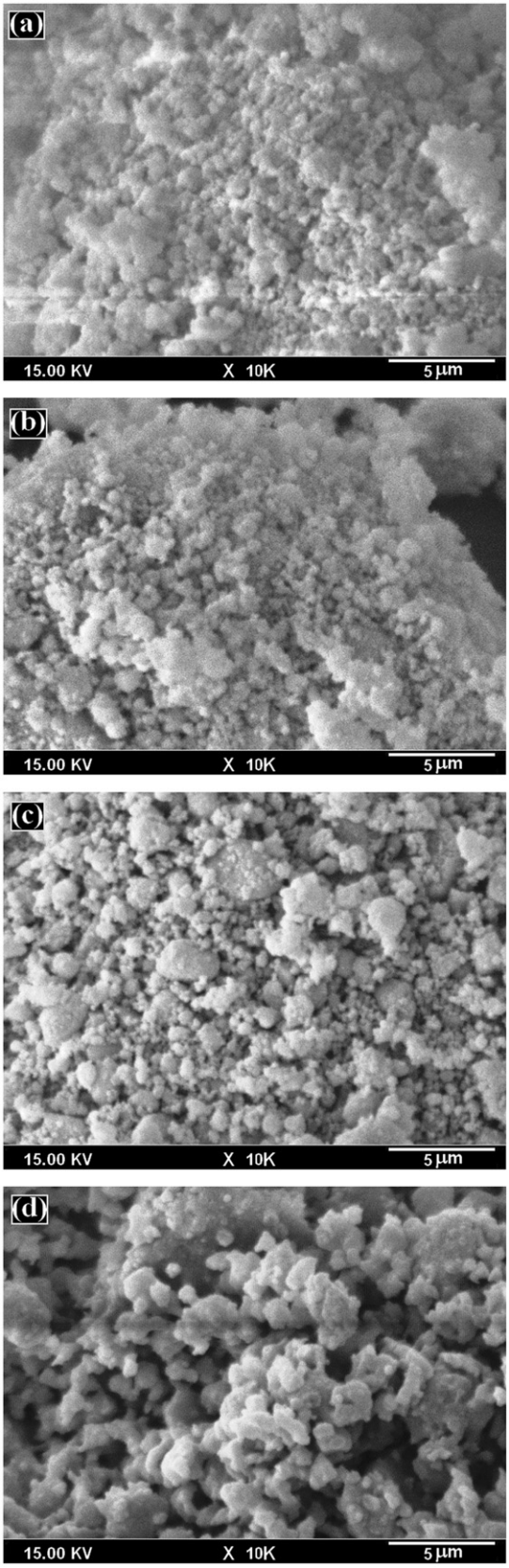

Fig. 5. SEM micrographs of the of the samples: (a) HAp/TiO_2–MgO after 10 h of milling, (b) HAp/$MgTiO_3$–MgO after 10 h of milling+heat treatment at 700 °C, (c) β-TCP/$MgTiO_3$–MgO after 10 h of milling+heat treatment at 900 °C, and (d) β-TCP/$MgTiO_3$–MgO after 10 h of milling+heat treatment at 1100 °C.

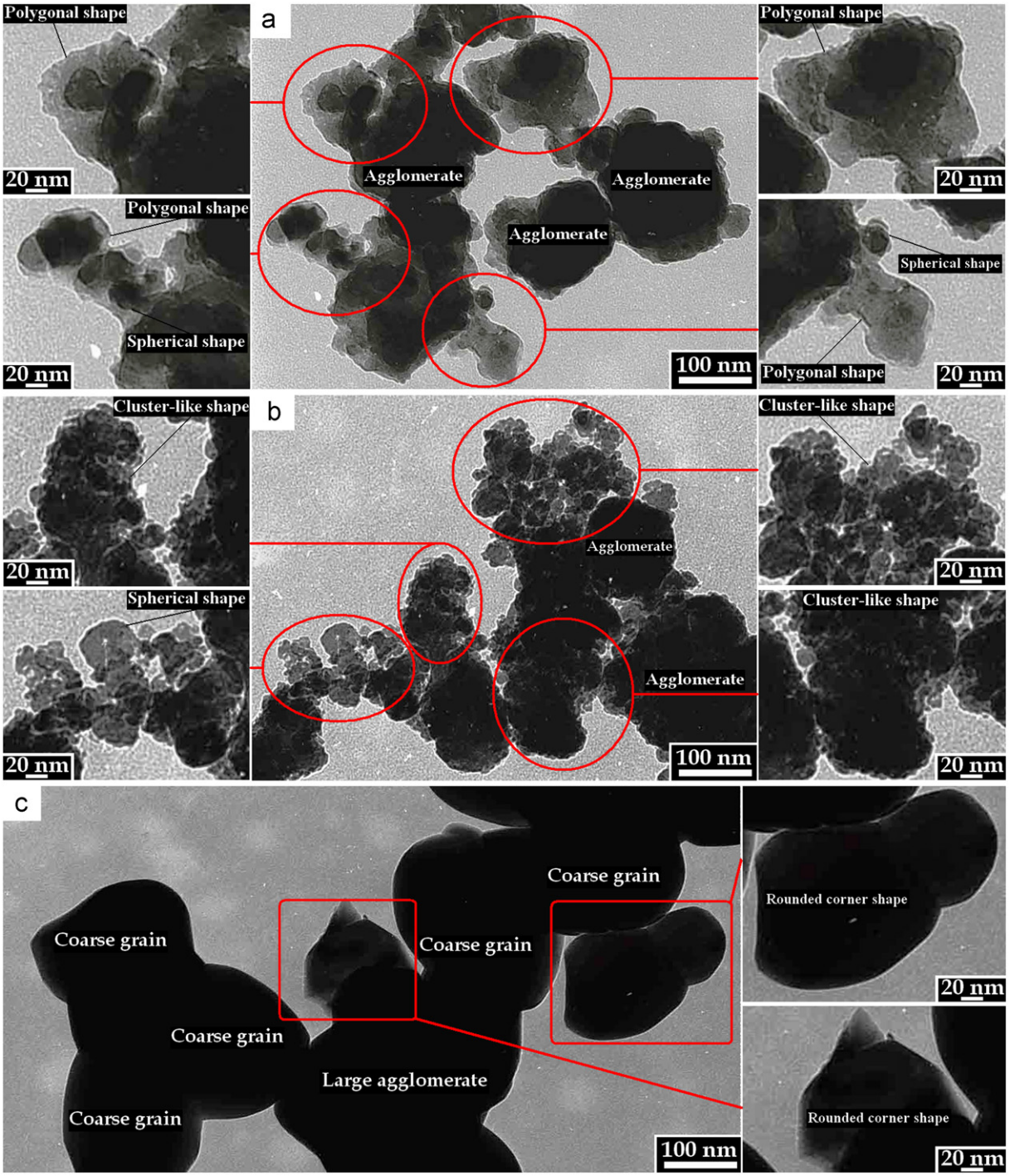

Fig. 6. TEM images of the samples: (a) HAp/TiO_2–MgO after 10 h of milling, (b) HAp/$MgTiO_3$–MgO after 10 h of milling + heat treatment at 700 °C, and (c) β-TCP/$MgTiO_3$–MgO after 10 h of milling + heat treatment at 1100 °C.

the formation of HAp/$MgTiO_3$–MgO and β-TCP/$MgTiO_3$–MgO composites with acceptable purity was confirmed in accordance with FT-IR results, as revealed from the X-ray profiles.

3.3. EDX analysis

Energy dispersive X-ray spectroscopy (EDX) has been performed to confirm that the obtained products from the proposed synthesis processes are HAp- and β-TCP-based composites. Fig. 4 represents the EDX results for HAp- and β-TCP-based composites which were synthesized after 10 h of milling and subsequent heat treatment in the range 700 − 1100 °C. EDX data showed that the main elements of the calcium phosphate-based composite nanopowders were calcium, phosphorus, oxygen, magnesium, and titanium. The EDX of HAp crystal, present in the HAp/MgO–TiO_2 composite exhibited a molar ratio Ca/P = 1.93,

whereas in the HAp/$MgTiO_3$–MgO composite the molar ratio of calcium to phosphorus was greater (Ca/P=2.87). These results suggest that the HAp crystals are closer to the expected value for the molar ratio of calcium to phosphorus ratio for the standard hydroxyapatite (Ca/P=1.67) [11] and commercial hydroxyapatite (2.38) [35], respectively. On the other hand, the Ca/P ratio for β-TCP in β-TCP/$MgTiO_3$–MgO composites was 1.28 and 2.50 at 900 and 1100 °C, respectively. Based on this results, the Ca/P ratio for β-TCP in β-TCP/$MgTiO_3$–MgO composite after 900 °C is closer to the standard β-TCP (Ca/P=1.5). In the case of β-TCP/$MgTiO_3$–MgO composite after 1100 °C, the increase in Ca/P ratio to more than 1.5 may be attributed to the formation of calcium phosphate compounds with lower Ca/P ratio than 1.5 which is in agreement with previous research [36]. It is noteworthy to mention that chemically stable contaminants were not detected due to the excessive adhesion of powders to the vial and balls.

3.4. SEM and TEM observations

According to the fact that the calcium phosphate based ceramics with appropriate morphological characteristics have better functions in biomedical applications [10], the morphological features as an important aspect of bioceramics were evaluated by using SEM and TEM techniques. Fig. 5 shows the SEM micrographs of the samples after milling and thermal treatment. As can be seen in Fig. 5(a), a very fine structure formed after 10 h of milling. After thermal treatment in the range 700 − 1100 °C (Fig. 5(b)–(d)), continuous evolution of the morphological features was appeared. The mean size of the powder particles increased after thermal treatment; however, only a slight change in particle size was observed in heat treated sample at 700 °C compared to the milled powder. After milling and subsequent thermal treatment at 700 °C, the products composed of fine particles with a mean particle size of about 482 and 510 nm, respectively (Fig. 5(a) and (b)). On the contrary, with increasing annealing temperature from 700 °C to 1100 °C the average of particle size enhanced. With increasing annealing temperature from 700 °C to 900 °C the powder particles became nearly equiaxed in shape with a mean particle size of about 1 μm (Fig. 5c). When the annealing temperature increased to 1100 °C grain growth happened and the mean particle size reached to about 1.5 μm (Fig. 5d). The SEM observations indicate that increasing the annealing temperature might assist grain growth due to the lack of any obstacle for particle growth.

Typical TEM images of calcium phosphate-based nanocomposites produced after 10 h of milling and subsequent thermal treatment in the range 700 − 1100 °C were shown in Fig. 6. From TEM observations, the particles exhibit high tendency to agglomerate. According to literature [37], when two adjacent primary particles collide, the coalescence may take place on the premise that these two particles share a common crystallographic orientation. Hence, two primary particles attach to each other and combine into a secondary one. Since the sizes of the secondary particles are still very small, it is reasonable that they will continue to collide and coalesce which may ultimately lead to the agglomeration. In Fig. 6(a), it can be seen that the agglomerates with an average size of about 185 nm formed after 10 h of milling which were consisted of mostly polyhedron like and spheroidal shape crystals with a mean size of about 40 nm. The agglomerates with mean size of about 322 nm were developed after thermal treatment at 700 °C. In this sample, the cluster-like shape particles composed of fine spheroidal shape crystals with a mean size of about 55 nm (Fig. 6a). It should be mentioned that chemical interactions at the contacting surface of crystals resulted in cluster-like shape aggregates which were composed of fine spheroidal shape crystals. This phenomenon is referred to the nature of milling process which originates through repeated welding, fracturing and re-welding of fine powder particles [26,27]. Also, Fig. 6(c) shows that after annealing at 1100 °C the abnormal grain growth occurred; so that the average size of grains with rounded corner shape was about 332 nm. These results were in agreement with SEM results.

The above-mentioned results suggest that the one-step mechanochemical process followed by thermal treatment is an effective route for producing nanostrutured calcium phosphate-based materials with appropriate structural features as well as morphological characteristics.

4. Conclusions

Novel calcium phosphate-based composite nanopowders with appropriate structural features as well as morphological characteristics were synthesized via one-step mechanochemical process and subsequent thermal treatment. According to XRD data, thermal annealing of the milled powders in the range 700–1100 °C resulted in the formation of HAp- and β-TCP-based nanocomposites with different structural features. The calculated amounts of crystallite size indicated that increasing of the annealing temperature might assist grain growth, although all the composite powders were in the nanosized range. According to the FT-IR results, the synthesized nanopowders had an acceptable purity. In addition, no chemically stable contaminants were detected due to the excessive adhesion of powders to the vial and balls. The SEM and TEM observations revealed that the sample annealed at 700 °C exhibited small grains with a mean size of about 55 nm, while the samples heat treated at higher temperatures ($\geq$ 900 °C) composed of coarse grains with an average size of about 332 nm. The results confirm that if an appropriate thermal treatment is selected after mechanochemical process, calcium phosphate-based nanocomposite with suitable characteristics can be obtained.

Acknowledgment

The authors are grateful to research affairs of Islamic Azad University, Najafabad Branch for supporting this research.

References

[1] Q. Xu, G.J. Lu, X.J. Bian, G.D. Jin, W. Wang, X.Y. Hu, Y. Wang, Zh. Yang, Calcium phosphate–gold nanoparticles nanocomposite for protein adsorption and mediator-free H_2O_2 biosensor construction, Materials Science and Engineering C 32 (2012) 470–477.

[2] A. Farzadi, M. Solati-Hashjin, F. Bakhshi, A. Aminian, Synthesis and characterization of hydroxyapatite/β-tricalcium phosphate nanocomposites using microwave irradiation, Ceramics International 37 (2011) 65–71.

[3] O.D. Schneider, A. Stepuk, D. Mohn, N.A. Luechinger, K. Feldman, W.J. Stark, Light-curable polymer/calcium phosphate nanocomposite glue for bone defect treatment, Acta Biomaterialia 6 (2010) 2704–2710.

[4] S.J. Kalita, A. Bhardwaj, H.A. Bhatt, Nanocrystalline calcium phosphate ceramics in biomedical engineering, Materials Science and Engineering C 27 (2007) 441–449.

[5] K.P. Sanosh, M.C. Chu, A. Balakrishnan, T.N. Kim, S.J. Cho, Sol–gel synthesis of pure nano sized β-tricalcium phosphate crystalline powders, Current Applied Physics 10 (2010) 68–71.

[6] D. Choi, P.N. Kumta, Mechano-chemical synthesis and characterization of nanostructured β-TCP powder, Materials Science and Engineering C 27 (2007) 377–381.

[7] S. Pushpakanth, B. Srinivasan, B. Sreedhar, T.P. Sastry, An in situ approach to prepare nanorods of titania hydroxyapatite (TiO_2-HAp) nanocomposite by microwave hydrothermal technique, Materials Chemistry and Physics 107 (2008) 492–498.

[8] M. Fini, L. Savarino, N.N. Aldini, L. Martini, G. Giavaresi, G. Rizzi, D. Martini, A. Ruggeri, A. Giunti, R. Giardino, Biomechanical and histomorphometric investigations on two morphologically differing titanium surfaces with and without fluorohydroxyapatite coating: an experimental study in sheep tibiae, Biomaterials 24 (2003) 3183–3192.

[9] Y. Chen, X. Miao, Thermal and chemical stability of fluorohydroxyapatite ceramics with different fluorine contents, Biomaterials 26 (2005) 1205–1210.

[10] B. Nasiri-Tabrizi, P. Honarmandi, R. Ebrahimi-Kahrizsangi, P. Honarmandi, Synthesis of nanosize single-crystal hydroxyapatite via mechanochemical method, Materials Letters 63 (2009) 543–546.

[11] I. Cacciotti, A. Bianco, M. Lombardi, L. Montanaro, Mg-substituted hydroxyapatite nanopowders: synthesis, thermal stability and sintering behavior, Journal of the European Ceramic Society 29 (2009) 2969–2978.

[12] R. Ebrahimi-Kahrizsangi, B. Nasiri-Tabrizi, A. Chami, Characterization of single-crystal fluorapatite nanoparticles synthesized via mechanochemical method, Particuology 9 (2011) 537–544.

[13] A. Fahami, R. Ebrahimi-Kahrizsangi, B. Nasiri-Tabrizi, Mechanochemical synthesis of hydroxyapatite/titanium nanocomposite, Solid State Sciences 13 (2011) 135–141.

[14] Y.W. Gu, N.H. Loh, K.A. Khor, S.B. Tor, P. Cheang, Spark plasma sintering of hydroxyapatite powders, Biomaterials 23 (2002) 37–43.

[15] B. Viswanath, N. Ravishankar, Interfacial reactions in hydroxyapatite/alumina nanocomposites, Scripta Materialia 55 (2006) 863–866.

[16] R.R. Rao, T.S. Kannan, Synthesis and sintering of hydroxyapatite–zirconia composites, Materials Science and Engineering C 20 (2002) 187–193.

[17] S. Nath, R. Tripathi, B. Basu, Understanding phase stability, microstructure development and biocompatibility in calcium phosphate–titania composites, synthesized from hydroxyapatite and titanium powder mixture, Materials Science and Engineering C 29 (2009) 97–107.

[18] H.H. Jin, S.H. Min, Y.K. Song, H.Ch. Park, S.Y. Yoon, Degradation behavior of poly(lactide-co-glycolide)/β-TCP composites prepared using microwave energy, Polymer Degradation and Stability 95 (2010) 1856–1861.

[19] H. Cao, N. Kuboyama, A biodegradable porous composite scaffold of PGA/β-TCP for bone tissue engineering, Bone 46 (2010) 386–395.

[20] H. Hu, X. Liu, Ch. Ding, Preparation and in vitro evaluation of nanostructured TiO_2/TCP composite coating by plasma electrolytic oxidation, Journal of Alloys and Compounds 498 (2010) 172–178.

[21] I. Mobasherpour, M. Solati-Hashjin, A. Kazemzadeh, Synthesis of nanocrystalline hydroxyapatite by using precipitation method, Journal of Alloys and Compounds 430 (2007) 330–333.

[22] N. Kivrak, A.C. Tas, Synthesis of calcium hydroxyapatite–tricalcium phosphate composite bioceramic powders and their sintering behavior, Journal of the American Ceramic Society 81 (1998) 2245–2252.

[23] F. Liu, F. Wang, T. Shimizu, K. Igarashi, L. Zhao, Hydroxyapatite formation on oxide films containing Ca and P by hydrothermal treatment, Ceramics International 32 (2006) 527–531.

[24] C.C. Silva, A.G. Pinheiro, M.A.R. Miranda, J.C. Goes, A.S.B. Sombra, Structural properties of hydroxyapatite obtained by mechanosynthesis, Solid State Sciences 5 (2003) 553–558.

[25] A. Balamurugan, S. Kannan, S. Rajeswari, Bioactive sol–gel hydroxyapatite surface for biomedical application—in vitro study, Trends in Biomaterials and Artificial Organs 16 (2002) 18–20.

[26] C. Suryanarayana, Mechanical alloying and milling, Progress in Materials Science 46 (2001) 1–184.

[27] C.L. De Castro, B.S. Mitchell, Synthesis functionalization and surface treatment of nanoparticles, in: M.I. Baraton (Ed.), Nanoparticles from Mechanical Attrition, American Scientific Publishers, Stevenson Ranch, CA, 2002, pp. 1–14.

[28] E. Landi, A. Tampieri, G. Celotti, S. Sprio, Densification behavior and mechanisms of synthetic hydroxyapatites, Journal of the European Ceramic Society 20 (2000) 2377–2387.

[29] Y.T. Sul, Osseoinductive Magnesium-Titanate Implant and Method of Manufacturing the Same. United State Patent, Patent no.: US 7,452,566 B2, 2008.

[30] J. Venkatesan, S.K. Kim, Effect of temperature on isolation and characterization of hydroxyapatite from tuna (thunnus obesus) bone, Materials 3 (2010) 4761–4772.

[31] A.S.F. Alqap, I. Sopyan, Low temperature hydrothermal synthesis of calcium phosphate ceramics: effect of excess Ca precursor on the phase behaviour, Indian Journal of Chemistry 48A (2009) 1492–1500.

[32] K.P. Sanosh, M.C. Chu, A. Balakrishnan, Y.J. Lee, T.N. Kim, S.J. Cho, Synthesis of nano hydroxyapatite powder that simulate teeth particle morphology and composition, Current Applied Physics 9 (2009) 1459–1462.

[33] J.G. Baek, T. Isobe, M. Senna, Mechanochemical effects on the precursor formation and microwave dielectric characteristics of $MgTiO_3$, Solid State Ionics 90 (1996) 269–279.

[34] M.K. Suresh, J.K. Thomas, H. Sreemoolanadhan, C.N. George, A. John, S. Solomon, P.R.S. Wariar, J. Koshy, Synthesis of nanocrystalline magnesium titanate by an auto-igniting combustion technique and its structural, spectroscopic and dielectric properties, Materials Research Bulletin 45 (2010) 761–765.

[35] C.C. Silva, A.G. Pinheiro, S.D. Figueiro, J.C. Goes, J.M. Sasaki, M.A.R. Miranda, A.S.B. Sombra, Piezoelectric properties of collagen–nanocrystalline hydroxyapatite composites, Journal of Materials Science 37 (2002) 2061–2070.

[36] M. Kitamura, Ch. Ohtsuki, Sh.I. Ogata, M. Kamitakahara, M. Tanihara, Microstructure and bioresorbable properties of α-TCP Ceramic porous body fabricated by direct casting method, Materials Transactions 45 (2004) 983–988.

[37] J. Zhang, Zh. Lin, Y. Lan, G. Ren, D. Chen, F. Huang, M. Hong, A multistep oriented attachment kinetics: coarsening of ZnS nanoparticle in concentrated NaOH, Journal of the American Chemical Society 128 (2006) 12981–12987.